Activity of Silica-Rich Hydrothermal Fluid and Its Impact on Deep Dolomite Reservoirs in the Sichuan Basin, Southern China

ZHU Dongya[1, 2, *], ZHANG Dianwei[1, 2], LIU Quanyou[1, 2], JIN Zhijun[1, 2] and HE Zhiliang[1, 2]

1 *State Key Laboratory of Shale Oil and Gas Enrichment Mechanisms and Effective Development, Beijing 100083, China*

2 *Petroleum Exploration and Production Research Institute of SINOPEC, Laboratory of Structural and Sedimentological Reservoir Geology, Beijing 100083, China*

Abstract: Well-developed dissolution pores occur in the dolomites of the Sinian Dengying Formation, which is an important oil and gas reservoir layer in the Sichuan Basin and adjacent areas in southern China. The pores are often filled with quartz, and some dolomites have been metasomatically altered to siliceous chert. Few studies have documented the characteristics, source or origin of silica-rich fluids and their effects on the dolomite reservoir. The peak homogenisation temperatures (T_h) of fluid inclusions in pore-filling quartz are between 150°C and 190°C, with an average of 173.7°C. Gases in the inclusions are mainly composed of CO_2, CH_4 and N_2. Compared with host dolomite, pore-filling quartz and metasomatic chert contain higher amounts of Cr, Co, Mo, W and Fe, with average concentrations of 461.58, 3.99, 5.05, 31.43 and 6666.83 ppm in quartz and 308.98, 0.99, 1.04, 13.81 and 4703.50 ppm in chert, respectively. Strontium levels are lower than that in the host dolomite, with average concentrations in quartz and chert of 4.81 and 11.06 ppm, respectively. Rare earth element compositions in quartz and chert display positive Eu anomalies with a maximum δEu of 5.72. The δD_{SMOW} values of hydrogen isotopes in water from quartz inclusions vary from −85.1‰ to −53.1‰ with an average of −64.3‰, whereas the $\delta^{18}O_{SMOW}$ values range from 7.2‰ to 8.5‰ with an average of 8.2‰. The average $^{87}Sr/^{86}Sr$ ratios in quartz and chert are 0.711586 and 0.709917, respectively, which are higher than that in the host dolomite. The fluid inclusions, elemental and isotopic compositions demonstrate that the formation of quartz and chert was related to silica-rich hydrothermal fluid and that the fluid was the deep circulation of meteoric water along basement faults. Interactions with silica-rich hydrothermal fluids resulted in densification of dolomite reservoirs in the Dengying Formation through quartz precipitation and siliceous metasomatism. However, it increased the resistance of the host dolomite to compaction, improving the ability to maintain reservoir spaces during deep burial. Evidence for silica-rich hydrothermal activity is common in the Yangtze Platform and Tarim Basin and its influence on deep dolomite reservoirs should be thoroughly considered.

Key words: Dengying Formation dolomite, silica-rich hydrothermal fluid, quartz, rare earth element, Sichuan Basin

1 Introduction

Dissolution and precipitation of carbonate minerals by various fluids are important processes that influence the development of carbonate reservoirs. Ca^{2+}/Mg^{2+}- and CO_2/CO_3^{2-}-rich fluids are responsible for the dissolution and precipitation of calcite and dolomite in carbonate rocks and are crucial for reservoir development. A number of studies have investigated the functions of Ca^{2+}/Mg^{2+}- and CO_2/CO_3^{2-}-rich fluids. For example, the dissolution of calcite by acidic fluids (such as organic acids, CO_2 and H_2S) related to hydrocarbon generation during the maturation of organic matter (Mazzullo and Harris, 1992; Ehrenberg, 2006; Qian Yixiong et al., 2006; Jin et al., 2009) and thermochemical sulphate reduction (TSR) process (Liu et al., 2013; Hao et al., 2015; Liu et al., 2016)

* Corresponding author. E-mail: zhudy.syky@sinopec.com

and dissolution and precipitation of calcite and dolomite by hydrothermal fluids (Lavoie et al., 2010; Davies and Smith, 2006; Jin et al., 2006; Liu Shugen et al., 2008; Zhang et al., 2009; Breesch et al., 2010; Liu Shugen et al., 2014; Zhu Dongya et al., 2017; Zhu et al., 2015; Huang Keke et al., 2016; Shen Anjiang et al., 2017) have been investigated in detail.

The dolomites of the Sinian Dengying Formation (Z_2dy) constitute an important oil and gas reservoir layer in the Sichuan Basin and adjacent areas in southern China. High-quality dolomite reservoirs and large amounts of natural gas have been found in the Dengying Formation in the Weiyuan and Ziyang gas fields (Jin Zhijun, 2005; Wei et al., 2008), as well as in recently drilled wells such as Gaoshi 1, Jinshi 1 and Lin 1. In outcrops and drill cores, dissolution pores in the dolomite reservoir are often filled with drusy quartz and a small proportion of dolomites have additionally been metasomatically altered to siliceous chert. The alteration of carbonate reservoirs by silica-rich fluids has been commonly observed (Chen Yongquan et al., 2010; Liu Shugen et al., 2014; Yin Xueqin et al., 2015), however, at present, the characteristics, origin and source of the silica-rich fluids as well as their impact on deep dolomite reservoirs have not yet been investigated.

In this study, we performed petrographic analyses, along with compositional analyses of carbon, oxygen and strontium isotopes, trace elements, rare earth elements and fluid inclusions in pore-filling quartz and metasomatic chert samples and investigated the characteristics and formation of silica-rich fluids and their impact on the dolomite reservoir. The results obtained from this study will lead to better understanding of the mechanisms involved in the development of deep dolomite reservoirs in the Dengying Formation.

2 Geological Settings

After decades of oil and gas exploration, high-quality deep dolomite reservoirs have been discovered in the Sinian Dengying Formation from several wells and outcrops in the Sichuan Basin and surrounding areas in southern China (Fig. 1). This formation produces large amounts of natural gas from the Weiyuan and Ziyang gas fields (Jin Zhijun, 2005; Liu Shugen et al., 2008; Wei et

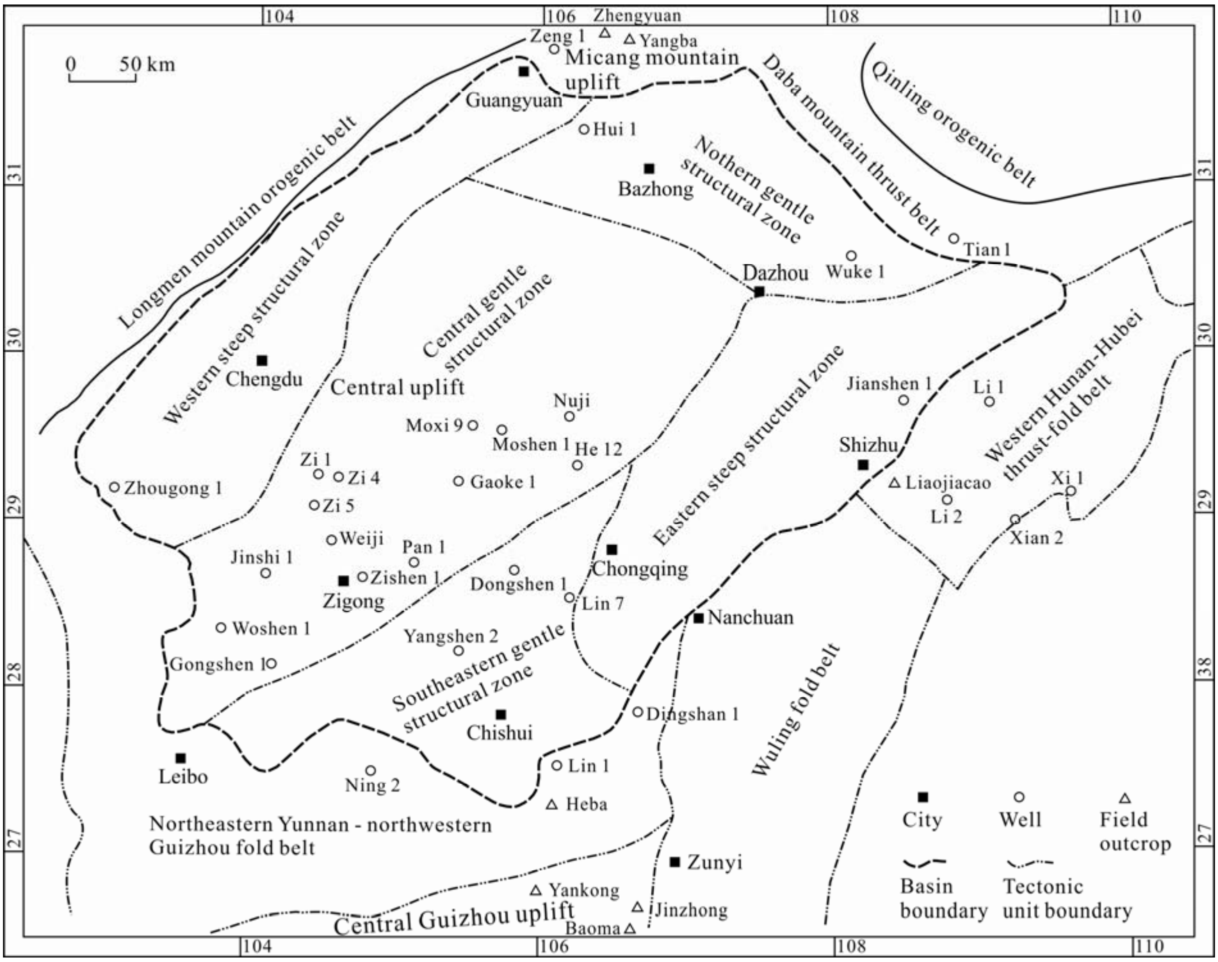

Fig. 1. Map showing tectonic units and locations of wells and field outcrops in the Sichuan Basin and surrounding areas, southern China.

al., 2008).

The Sinian Dengying Formation (Z_2dy) can be divided into four sections: Z_2dy^1, Z_2dy^2, Z_2dy^3 and Z_2dy^4. From the base of the formation upward, the Z_2dy^1 section mainly comprises siliciclastic rocks with dolomite interlayers; Z_2dy^2 is mainly dolomite with typical grape-shaped structures; Z_2dy^3 mainly comprises grey–brown and brown –yellow sandstone and black mudstone; Z_2dy^4 is mainly dolomite, often algal dolomite, oolitic dolomite or finely crystalline dolomite with siliceous interlayers. Below the Denying Formation lies the Doushantuo Formation (Z_1d), which is composed of epimetamorphic sandstone and carbonate rocks. The Dengying Formation is overlain by Lower Cambrian dark grey/black shales.

Due to the Tongwan movement during the late Sinian period, the Sichuan Basin and surrounding areas were uplifted; this caused widespread exposure of the dolomite in the Dengying Formation at ground level and led to karstification by meteoric water, producing dissolution pores that act as the main reservoir spaces. From the Paleozoic to Mesozoic periods, the Dengying Formation underwent continuous burial until the Yanshan–Xishan orogeny when strong compressional uplift occurred (Zhao Zongju et al., 2003; Li Shuangjian et al., 2011), resulting in uplift and denudation of the areas around the Sichuan Basin and a second period of exposure of the Dengying Formation at the Earth's surface.

The main hydrocarbon source rocks for the Sinian and Lower Paleozoic oil and gas reservoirs in the Sichuan Basin and surrounding areas are the black shales and mudstones in the Z_2dy^3 section and the Lower Cambrian units (Liu et al., 2011; Ni et al., 2014). These source rocks produced hydrocarbons during the middle and late stages of the Caledonian orogeny (Zhao Zongju et al., 2003; Li Shuangjian et al., 2011) and these hydrocarbons accumulated in the dolomite reservoirs of the Sinian Dengying Formation. From the late Paleozoic to the Mesozoic period, the dolomite reservoirs in the Sinian Dengying Formation experienced an extended period of burial and high temperatures, during which oil was thermally converted into carbonaceous bitumen with high reflectance (Zhu Dongya et al., 2013).

Two tectonic-hydrothermal events occurred in the Sichuan Basin and the adjacent upper Yangtze areas during the Sinian and Paleozoic periods: namely, the Xingkai *movement and Emei movement (*Liu Shugen et al., 2008) occurred during the Late Sinian to Early Cambrian period (Z_2–$Є_1$) and during the Middle Devonian to Middle Triassic period (D_2–T_2), respectively (Luo et al., 1981). Chen et al., (2009) found evidence for a siliceous hydrothermal event during the early Cambrian period. In the Sichuan Basin and the central Guizhou uplift, a prominent feature of this hydrothermal activity is the formation of a series of Pb, Zn and other MVT- and SEDEX-type metal deposits (Liu Shugen et al., 2008).

3 Samples and Methods

Quartz fillings in dissolution pores and metasomatic chert in the Dengying Formation dolomite were systematically sampled. For comparison, samples of the host dolomite near the pore-filling quartz and metasomatic chert were also collected. The sampling sites are shown in Fig. 1. Well-core samples were taken from the wells Jinshi 1 and Lin 1. Thin sections of the samples were observed under an optical microscope and analysed to obtain the fluid inclusion temperatures, laser Raman spectra, trace and rare earth element compositions and hydrogen, oxygen and strontium isotopic signatures.

Samples for thin section observations were doubly polished to about 0.03 mm thick, and those for fluid inclusion temperature measurements were about 0.2 mm thick. Microscopic observations of thin sections included determinations of the petrology, mineralogy and pore structures using a Leica DM4500 microscope. Fluid inclusion measurements were performed on a Linkam-TH600 heating-cooling stage. After temperature adjustment, the measurements were performed at an initial heating rate of 15°C/min, which was decreased to 1°C/min when the fluid inclusions were close to homogenisation. The precision of the temperature measurements is ±1°C.

The gas compositions of single fluid inclusions were identified with a Renishaw RM2000 Raman microprobe equipped with an argon ion laser (514.5 nm) and a charge-coupled device detector. A pure silicon standard (520 cm^{-1}) was used to calibrate the microprobe, and the stated peak positions are reproducible to within ±1cm^{-1}. The scanning range for the spectra was set to 0–4000 cm^{-1} with an accumulation time of 30 s for each scan.

For geochemical analyses, the samples (pore-filling quartz, metasomatic chert and host dolomite) were ground to pass through 20–40 mesh sieves, ultrasonically cleaned and dried. Particles of each phase were selected under a binocular stereo microscope, and the selected particles were then ground to a powder of <200 mesh for elemental and isotopic analyses.

Minor element and rare earth element compositions were determined using ICP-MS with a Yokogava PMS-200 instrument. Each powdered sample (40 mg) was placed in a dissolving jar with 3 mL (1+1) HNO_3. The jar was placed on an electrothermal plate to maintain a temperature of 120°C for an entire day, and then the temperature was increased to 150°C and maintained for another day. The solution was evaporated until almost dry.

Then, 2 mL (1+1) of HNO_3 was added and the jar was again placed on an electrothermal plate to maintain a temperature of 150°C for 2 h. Furthermore, the liquid was evaporated to 1 mL and the solution was transferred into a 50 mL PE bottle. For analysis, the solution was finally diluted to 20 mL using sub-boiling water.

For oxygen isotope analysis, 10–30 mg of dried sample was reacted with pure BrF_5 at temperatures of 550–700°C to generate oxygen. The oxygen generated was reacted with carbon at 700°C with a platinum catalyst to generate CO_2 for isotope determinations in a MAT 251 gas isotope mass spectrometer. The analytical precision was 0.2‰.

For hydrogen isotope analysis, the separated quartz minerals were dried and gradually evacuated and heated under vacuum to remove water from secondary inclusions, and then heated to 600°C to rupture the inclusions. The water released was collected, condensed, purified and replaced with zinc to generate H_2 for mass spectrometric analysis.

Strontium isotope analysis was performed on a Finnigan MAT Triton TI instrument. About 100 mg of sample powder was placed in a dissolving jar and 2 mL of 6M HCl was added. The sample was dissolved for 24 h at a temperature range of 100–110°C. Ion chromatography was employed to separate the strontium isotopes. Using HCl as an eluant, an AG 50W-X12 200–400 mesh ion resin produced by Bia-Rad Coop. of USA was used to separate and enrich strontium isotopes. The measured $^{87}Sr/^{86}Sr$ values were adjusted according to a mass fractionation standard value of $^{87}Sr/^{86}Sr$ = 0.1194. The average analysed $^{87}Sr/^{86}Sr$ value of the NBS987 standard sample was 0.710273 ± 0.000012.

Fluid inclusion thermometry, laser Raman spectroscopy and trace and rare earth element analyses were conducted in the State Key Laboratory of Ore Deposit at Nanjing University, and hydrogen, oxygen and strontium isotopes were analysed at the Institute of Geology and Geophysics at the Chinese Academy of Sciences.

4 Results

4.1 Petrographic characteristics

A large number of dissolution pores can be observed in the dolomite of the Sinian Dengying Formation. The pore sizes generally range from 1 to 3 mm and can be as large as 3 cm in diameter (Figs. 2a–d, Figs. 3a–b). Dissolution pores filled with dolomite, quartz and bitumen were observed. The pore-filling dolomite includes two types: fibrous radial dolomite on the pore walls and coarse crystalline dolomite in the pore interiors (Figs. 2a, 2b and 2d, Figs. 3a and 3b). The coarse crystalline dolomite is typically rhombus- or saddle-shaped, a few mm in size and is mostly white (Fig. 2d). The coarse crystalline dolomite is generally characterised by curved crystal planes and wavy extinction.

Pore-filling quartz occurs as single long crystals or drusy crystals in pores, with sizes generally around a few mm to 1 cm (Figs. 2a–d). Pore-filling bitumen appears as black scales or spheres with a high degree of evolution (Fig. 2d). The reflectance of the bitumen (Rb) can be as high as 5.3% (Zhu Dongya et al., 2013).

Our observations revealed that some very fine/fine crystalline dolomite and algal/granular dolomite were metasomatically converted into chert by silica-rich hydrothermal fluids. Metasomatism in the very fine crystalline dolomite produced cryptocrystalline or fine-grained crystalline chert with ghost structures of laminar dolomite (Figs. 2e–f, Figs. 3c–d). Metasomatism in the algal or granule dolomite generated fine-to-medium-grained crystalline chert with predominant granular ghost textures (Figs. 3e and 3f).

4.2 Fluid inclusions

The pore-filling quartz contains abundant fluid inclusions, which are mostly square, rectangular or circular in shape and typically 10–25 μm in size (Figs. 3g–h). These fluid inclusions are randomly distributed in the quartz crystals as primary fluid inclusions. Under excitation by 405 nm blue light, the inclusions generally do not fluoresce and are therefore interpreted to be pure brine inclusions without hydrocarbons.

Microthermometry results indicate that the homogenisation temperatures (T_h) of the fluid inclusions in quartz range from 115.7 to 228.3°C with an average of 173.7°C (based on 83 T_h data) and the peak of T_h ranges from 150 to 190°C (Fig. 4). The salinity of the fluid inclusions is between 7.9 and 26.3 wt% NaCl eq., with an average of 16.7 wt%NaCl eq. (based on 31 salinity data).

Laser Raman analyses indicate that the gases in the inclusions are mainly CO_2, CH_4 and N_2. Among these, inclusions in pore-filling quartz from Jz-3Qz contain CO_2 and N_2, whereas those from the well Lin 1 comprise CO_2, CH_4 and N_2 (Fig. 5).

4.3 Geochemical characteristics

4.3.1 Trace elements

Some differences in trace element compositions were found between the pore-filling quartz, metasomatic chert and host dolomite (Table 1; Fig. 6). The data indicate that quartz and chert have relatively high concentrations of Cr, Co, Mo, W and Fe, with average concentrations of 461.58, 3.99, 5.05, 31.43 and 6666.83 ppm in quartz, 308.98, 0.99, 1.04, 13.81 and 4703.50 ppm in chert and 10.71, 0.93,

Fig. 2. Photographs showing pore-filling quartz and metasomatic chert in the Sinian Dengying Formation of the Sichuan Basin and surrounding areas.

(a), Dissolution pore in dolomite was filled by FD, CD and Qz, Z_2dy^2, Yankong outcrop; (b), Dissolution pore in dolomite was filled by FD, CD and Qz, Z_2dy^4, well Jinshi 1; (c), Dissolution pore in dolomite was filled by Qz, Z_2dy^4, Liaojiacao outcrop; (d), Dissolution pore in dolomite was filled by FD, CD, Qz and Bn, Z_2dy^2, Baoma outcrop; Pores and fractures in quartz were filled by bitumen, demonstrating bitumen was formed later than quartz; (e), Metasomatic chert with ghost of laminar structure of dolomite, Z_2dy^2, Zhengyuan outcrop; (f), Metasomatic chert with ghost of laminar structure of dolomite, Z_2dy^4, Zhengyuan outcrop; HD, Host dolomite; FD, Fibrous radial dolomite filling along wall of pore in dolomite; CD, Coarse crystalline dolomite filling in pore; Qz, Pore-filling quartz; Bn, Bitumen.

0.11, 0.45 and 2972.67 ppm in host dolomite, respectively. However, quartz and chert have lower Sr concentrations than that of the host dolomite with average Sr concentrations in quartz, chert and dolomite of 5.14, 12.60 and 44.65 ppm, respectively.

4.3.2 Rare earth elements

Our analyses show that host dolomite contains relatively low concentrations of rare earth elements (∑REE), which range from 1.78 to 24.17 ppm with an average of 7.06 ppm (Table 2). The distribution pattern for the host dolomite displays an enrichment in middle rare earth elements as well as a generally negative Ce anomaly (Fig. 7), with an average δCe value of 0.56.

The rare earth element concentrations (∑REE) in pore-filling quartz are somewhat lower (0.68–3.28 ppm with an average of 1.74 ppm) than those in the host dolomite. Most samples display a positive Eu anomaly and a range of δEu values from 0.90 to 2.23 with an average of 1.16 (Table 2; Fig. 7).

Similarly to the pore-filling quartz, metasomatic chert contains low concentrations of rare earth elements (∑REE = 0.38–0.71 ppm with an average of 0.58 ppm). The metasomatic chert has a remarkable positive Eu anomaly. Two chert samples have δEu values of 3.00 and 5.72 (Table 2; Fig. 7).

4.3.3 Isotopes

The δD_{SMOW} values of water from fluid inclusions in pore-filling quartz range from −85.1‰ to −53.1‰ with an

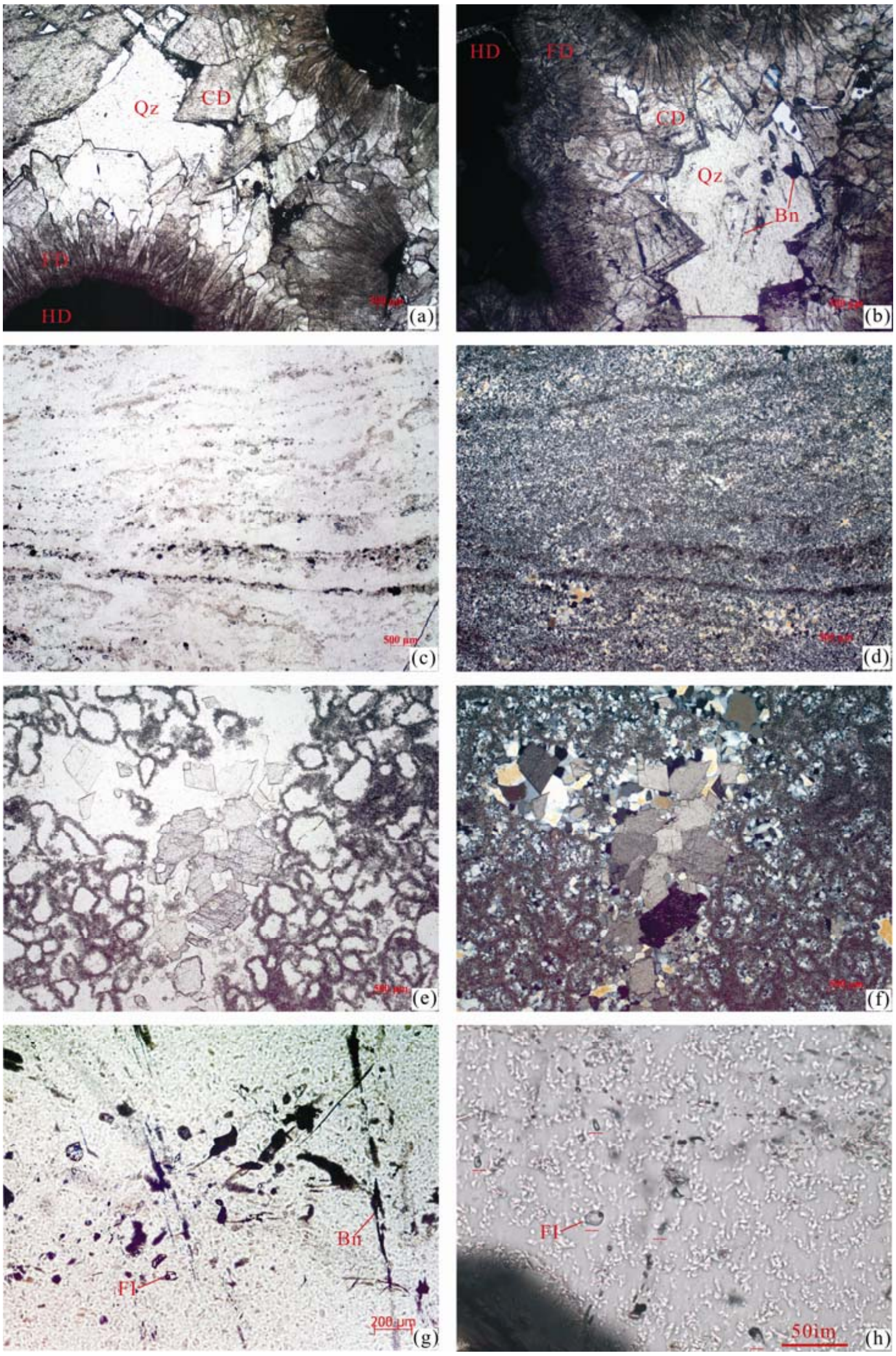

Fig. 3. Microphotographs of pore-filling quartz and metasomatic chert in Sinian Dengying Formation in the Sichuan Basin and surrounding areas.

(a), Dissolution pore in dolomite was filled by FD, CD and Qz, Z_2dy^2, Yankong outcrop, polarized light, ×25; (b), Dissolution pore in dolomite was filled by FD, CD, Qz and Bn, Z_2dy^2, Baoma outcrop, polarized light, ×25; Fractures in quartz were filled by bitumen, demonstrating bitumen was formed later than quartz; (c), Metasomatic chert with ghost of laminar structure of dolomite, Z_2dy^2, Zhengyuan outcrop, polarized light, ×25; (d), Metasomatic chert with ghost of laminar structure of dolomite, Z_2dy^2, Zhengyuan outcrop, cross polarized light, ×25; (e), Metasomatic chert with ghost of granular structure of dolomite, Z_2dy^4, Liaojiacao outcrop, polarized light, ×25; (f), Metasomatic chert with ghost of granular structure of dolomite, Z_2dy^4, Liaojiacao outcrop, cross polarized light, ×25; (g), Fractures in pore-filling quartz were filled by bitumen, demonstrating bitumen was formed later than quartz; Fluid inclusions in pore-filling quartz, Z_2dy^2, Baoma outcrop, polarized light, ×50; (h), Fluid inclusions in pore-filling quartz, Z_2dy^4, well Lin 1, polarized light, ×500; HD, Host dolomite; FD, Fibrous radial dolomite filling along wall of pore in dolomite; CD, Coarse crystalline dolomite filling in pore; Qz, Pore-filling quartz; Bn, Bitumen; FI, Fluid inclusion.

average of −64.3‰ (Table 3). The $\delta^{18}O_{SMOW}$ values for pore-filling quartz are between 19.5‰ and 23.9‰ with an average of 22‰. Based on homogenisation temperatures of the fluid inclusions and oxygen isotope equilibrium

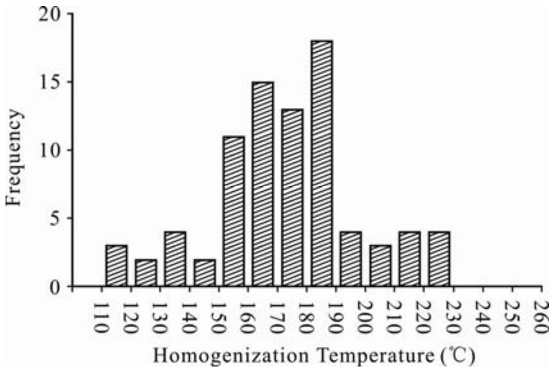

Fig. 4. Homogenization temperature of fluid inclusions in pore-filling quartz in the Sichuan Basin and surrounding areas.

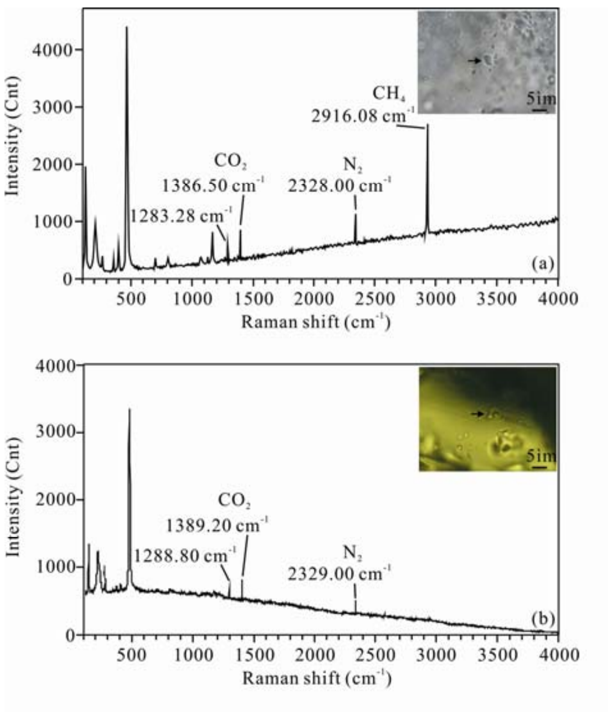

Fig. 5. Raman analyses for fluid inclusions in pore-filling quartz in the Sichuan Basin and surrounding areas.
(a), Gas compositons in fluid inclusion in quartz sample JZ-3Qz are CO_2, N_2 and CH_4; (b), Gas compositons in fluid inclusion in quartz sample from well Lin 1 are CO_2 and N_2.

fractionation equations between quartz and water, the $\delta^{18}O_{SMOW}$ values of the parent fluid of the precipitated quartz were calculated to range from 7.2‰ to 8.5‰ with an average of 8.2‰ (Table 3). The $\delta^{18}O_{SMOW}$ values of metasomatic chert vary from 20.7‰ to 28.1‰ with an average of 25.0‰. The metasomatic chert is thus isotopically heavier than the pore-filling quartz.

The $^{87}Sr/^{86}Sr$ ratios of the pore-filling quartz were determined to be between 0.709068 and 0.716564 with an average of 0.711586, those for metasomatic chert are between 0.708970 and 0.712375 with an average of 0.709917 and those for the host dolomite are between 0.708887 and 0.710583 with an average of 0.709496

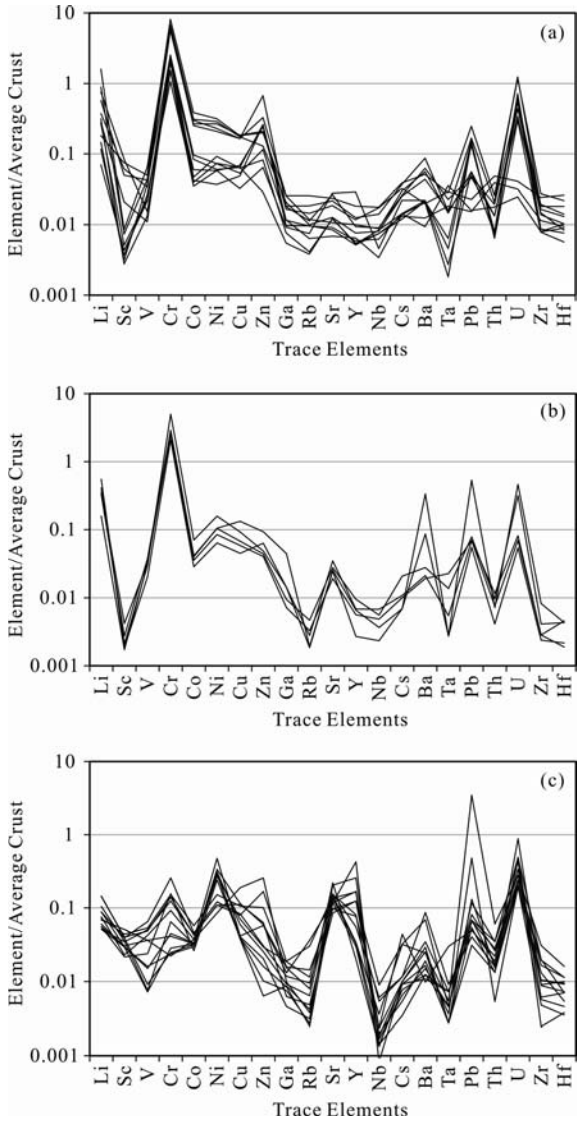

Fig. 6. Trace element distribution patterns for host dolomite, pore-filling quartz and metasomatic chert in the Sichuan Basin and surrounding areas.
(a), Pore-filling quartz; (b), Metasomatic chert; (c), Host dolomite.

(Table 3). Therefore, $^{87}Sr/^{86}Sr$ ratios are higher in the pore-filling quartz than in either the metasomatic chert or host dolomite.

5 Discussions

5.1 Diagenetic sequence

The Tongwan movement during the Late Sinian period produced uplift and surface exposure of the dolomite in the Sinian Dengying Formation in the Sichuan Basin and surrounding areas. The dolomite was consequently subjected to karstification by meteoric water. During the karst-forming process, numerous dissolution pores were formed in dolomite, which became the main reservoir spaces for oil and gas.

It is generally believed that the fibrous radial dolomite

Table 1 Concentrations of trace elements (in ppm) in host dolomite, pore-filling quartz and metasomatic chert in Sichuan basin and surrounding areas

Sample	Li	Sc	V	Cr	Co	Ni	Cu	Zn	Ga	Rb	Sr	Y	Nb	Cs	Ba
Pore-filling quartz															
YK-1Qz	2.98	0.112	2.96	175	1.49	2.97	0.78	4.7	0.146	0.431	9.01	0.579	0.055	0.057	8.59
BMG-2Qz	17.6	0.187	8.51	808	7.44	11.7	3.97	23.9	0.411	1.48	7.67	0.364	0.211	0.101	20
JZ-2Qz	1.28	0.081	3.44	127	1.05	1.88	1.17	19	0.154	0.556	2.73	0.103	0.089	0.031	8.3
JZ-3Qz	0.771	0.095	2.8	264	2.09	3.07	1.55	19.1	0.183	0.553	2.95	0.118	0.075	0.037	8.54
HB-3Qz	9.82	0.161	5.66	726	6.28	10.7	3.98	49	0.291	1.07	6.99	0.25	0.168	0.096	33.9
YK-6Qz	1.61	0.069	4.84	301	2.42	3.72	1.28	8.46	0.185	0.369	2.23	0.129	0.041	0.036	7.98
YK-7Qz	2	1.64	6.55	972	9.65	16.1	4.36	14.6	0.404	0.683	3.46	0.2	0.105	0.077	21.7
BMG-2Qz	6.27	1.1	5.56	777	7.78	14.7	4.2	9.4	0.33	0.578	4.1	0.152	0.096	0.065	17
BMG-3Qz	4.11	1.35	4.43	669	6.67	13.6	4.45	15.2	0.286	0.652	8.64	0.186	0.108	0.067	24.5
LJC-1Qz	8.29	1.87	1.99	181	0.871	2.95	1.65	17.7	0.264	0.832	6.06	0.234	0.206	0.084	7.71
LJC-8Qz	3.47	0.061	1.74	300	1.17	4.69	1.52	5.98	0.122	0.239	3.91	0.109	0.089	0.034	4.82
LJC-9Qz	3.08	0.461	1.44	239	0.986	3.75	1.54	2.09	0.087	0.221	3.97	0.106	0.1	0.037	3.65
Average	5.107	0.599	4.160	461.583	3.991	7.486	2.538	15.761	0.239	0.639	5.143	0.211	0.112	0.060	13.891
Metasomatic chert															
LJC-2C	1.74	0.038	4.19	302	0.891	4.3	1.4	2.94	0.115	0.19	6.25	0.112	0.058	0.026	7.51
LJC-6C	3.85	0.092	4.27	343	1.03	5.3	1.63	3.23	0.151	0.272	9.04	0.19	0.067	0.054	10.9
LJC-13C	4.5	0.046	3.92	594	1.76	8.07	2.22	3.55	0.227	0.161	11.3	0.136	0.081	0.028	8.29
ZY-7C	3.65	0.06	4.94	342	0.996	5.33	3.17	6.78	0.711	0.111	8.3	0.132	0.044	0.018	131
ZY-9C	6.05	0.041	2.67	250	0.717	3.25	1.08	4.6	0.227	0.107	8.01	0.054	0.028	0.018	33.7
YB-7C	1.25	0.461	7.15	22.9	0.554	10.9	1.16	3.59	0.146	0.242	32.7	0.151	0.028	0.024	5.51
Average	3.507	0.123	4.523	308.983	0.991	6.192	1.777	4.115	0.263	0.181	12.600	0.129	0.051	0.028	32.818
Host dolomite															
HB-3	0.833	0.507	5.54	11	0.929	4.33	4.52	18.8	0.157	0.22	44	0.662	0.024	0.014	7.4
YK-1	0.561	0.762	6.55	14.8	1.08	5.52	2.69	4.62	0.1	0.28	27.6	2.48	0.028	0.026	9.83
YK-2	0.787	0.963	6.96	18.1	1.43	7.74	2.53	7.35	0.252	0.832	31.5	2.46	0.108	0.084	26.8
YK-4	1.59	0.865	8.45	30.5	1.14	6.16	1.98	2.23	0.189	0.554	31.7	1.54	0.065	0.03	33.9
BMG-1	1.58	0.877	6.34	16.6	1.07	5.6	1.91	12.2	0.295	0.665	50.9	1.1	0.073	0.03	13.5
YB-11	1.15	0.774	1	7.72	0.8	13.9	1.69	2.15	0.301	1.76	47.4	0.681	0.043	0.083	9.47
Ljc-3	0.565	0.649	0.947	3.37	0.816	14.5	0.972	1.49	0.073	0.182	66.6	5.15	0.017	0.02	4.83
Ljc-6	0.751	1.12	4.76	2.63	0.932	24.3	1	4.21	0.209	2.11	38.4	3.35	0.028	0.114	3.81
Ljc-7	0.662	0.648	2.1	2.82	0.743	14.9	0.924	1.17	0.136	0.143	44.3	3.29	0.02	0.017	5.87
Ljc-17	0.611	0.476	3.13	18.5	0.656	12.3	0.923	0.74	0.121	0.157	38.8	0.6	0.017	0.009	4.83
LJC-4	0.973	0.65	1.97	5.29	0.832	15.9	1.41	1.85	0.147	0.373	49.8	1.61	0.022	0.024	6.42
LJC-10	0.97	0.858	1.2	2.95	0.791	14.8	0.903	0.465	0.139	0.243	37.8	8.54	0.01	0.024	4.22
ZY-5	0.608	0.668	4.75	4.89	0.812	17.2	2.75	4.32	0.245	0.46	71.6	0.401	0.016	0.026	11.4
Average	0.895	0.755	4.131	10.705	0.925	12.088	1.862	4.738	0.182	0.614	44.646	2.451	0.036	0.039	10.945
Average Crust*	11	22	131	119	25	51	24	73	16	58	325	20	12	2.6	390

Sample	Ta	Pb	Th	U	Zr	Hf	Mo	Cd	In	Sb	W	Fe
Pore-filling quartz												
YK-1Qz	0.003	0.696	0.042	0.784	0.97	0.033	1.66	0.01	0.004	0.154	9.72	1678
BMG-2Qz	0.031	3.11	0.144	1.66	3.35	0.081	8.79	0.02	0.013	0.532	52.7	8156
JZ-2Qz	0.007	1.93	0.038	1.02	1.07	0.028	1.39	0.006	0.004	0.051	6.8	945
JZ-3Qz	0.005	1.67	0.044	0.891	1.69	0.038	2.65	0.005	0.005	0.126	15.2	2213
HB-3Qz	0.017	2.13	0.116	1.76	2.23	0.067	8.23	0.015	0.007	0.211	49.9	7667
YK-6Qz	0.002	1.88	0.036	0.427	0.956	0.021	3.03	0.015	0.003	0.126	17.1	2479
YK-7Qz	0.016	0.705	0.074	0.627	2.02	0.048	12.6	0.02	0.001	0.259	71.1	14629
BMG-2Qz	0.017	0.586	0.074	0.484	1.81	0.031	9.9	0.001	0.003	0.362	57.9	11870
BMG-3Qz	0.025	0.603	0.108	0.782	2.38	0.052	8.4	0.022	0.002	0.307	43.7	9786
LJC-1Qz	0.032	0.285	0.272	0.058	2.98	0.096	1.23	0.029	0.005	0.072	13.6	8563
LJC-8Qz	0.02	0.192	0.219	0.045	1.4	0.035	1.37	0.009	0.002	0.111	21.6	5436
LJC-9Qz	0.039	0.2	0.099	0.035	0.978	0.038	1.38	0.001	0.002	0.099	17.8	6580
Average	0.018	1.166	0.106	0.714	1.820	0.047	5.053	0.013	0.004	0.201	31.427	6666.833
Metasomatic chert												
LJC-2C	0.025	0.878	0.065	0.116	0.35	0.017	1.08	0.009	0.001	0.085	14.4	3653
LJC-6C	0.015	0.987	0.054	0.455	0.506	0.016	1.14	0.013	0.002	0.124	16	8326
LJC-13C	0.006	0.87	0.042	0.099	0.348	0.007	2.05	0.013	0.003	0.118	27.3	2510
ZY-7C	0.003	6.72	0.04	0.654	1.01	0.016	1.2	0.021	0.002	0.105	13.1	1369
ZY-9C	0.003	0.692	0.023	0.077	0.293	0.008	0.706	0.011	0.001	0.056	10.9	6540
YB-7C	0.007	0.643	0.035	0.159	0.709	0.015	0.086	0.008	0.002	0.025	1.13	5823
Average	0.010	1.798	0.043	0.260	0.536	0.013	1.044	0.013	0.002	0.086	13.805	4703.500
Host dolomite												
HB-3	0.004	6.04	0.03	0.276	0.587	0.013	0.087	0.273	0.004	0.105	0.374	2852
YK-1	0.003	0.393	0.075	0.272	1.62	0.02	0.039	0.043	0.002	0.044	0.378	2715
YK-2	0.005	0.821	0.158	0.344	2.41	0.042	0.162	0.051	0.004	0.075	0.565	3549
YK-4	0.01	0.51	0.09	0.286	1.28	0.034	0.248	0.008	0.005	0.065	1.46	3046
BMG-1	0.008	0.645	0.106	0.326	2.04	0.042	0.101	0.018	0.003	0.186	0.411	3171
YB-11	0.006	43.8	0.338	0.395	3.79	0.059	0.262	0.011	0.002	0.067	0.57	2503
Ljc-3	0.005	0.852	0.196	0.698	0.703	0.017	0.104	0.011	0.001	0.038	0.231	2859
Ljc-6	0.033	0.619	0.123	0.48	1.08	0.027	0.139	0.021	0.001	0.059	0.125	2942

Table 1 (Continued)

Sample	Ta	Pb	Th	U	Zr	Hf	Mo	Cd	In	Sb	W	Fe
Ljc-7	0.005	1.47	0.194	0.399	0.756	0.026	0.042	0.013	0.001	0.031	0.151	3356
Ljc-17	0.008	0.858	0.096	0.629	0.3	0.014	0.093	0.009		0.025	1.05	3024
LJC-4	0.003	0.682	0.074	0.701	2.46	0.026	0.036	0.04	0.001	0.03	0.179	1856
LJC-10	0.008	1.02	0.146	0.285	1.29	0.035	0.023	0.008	0.002	0.031	0.112	2015
ZY-5	0.003	1.66	0.086	1.25	1.11	0.037	0.104	0.079	0.002	0.013	0.236	2501
Average	0.008	4.567	0.132	0.488	1.494	0.030	0.111	0.045	0.002	0.059	0.449	2972.667

*Average crust, Taylor and McLennan (1985).
Samples with name starting with "YK-" were collected from Yankong field outcrops, "BMG-" from Baoma field ourcrop, "JZ-" from Jinzhong field outcrop, "HB-" from Heba outcrop, "LJC-" from Liaojiacao field outcrop, "ZY-" from Zhengyuan field outcrop, and "YB-" from Yangba field outcrop. See Fig. 1 for locations of the field outcrops and wells.

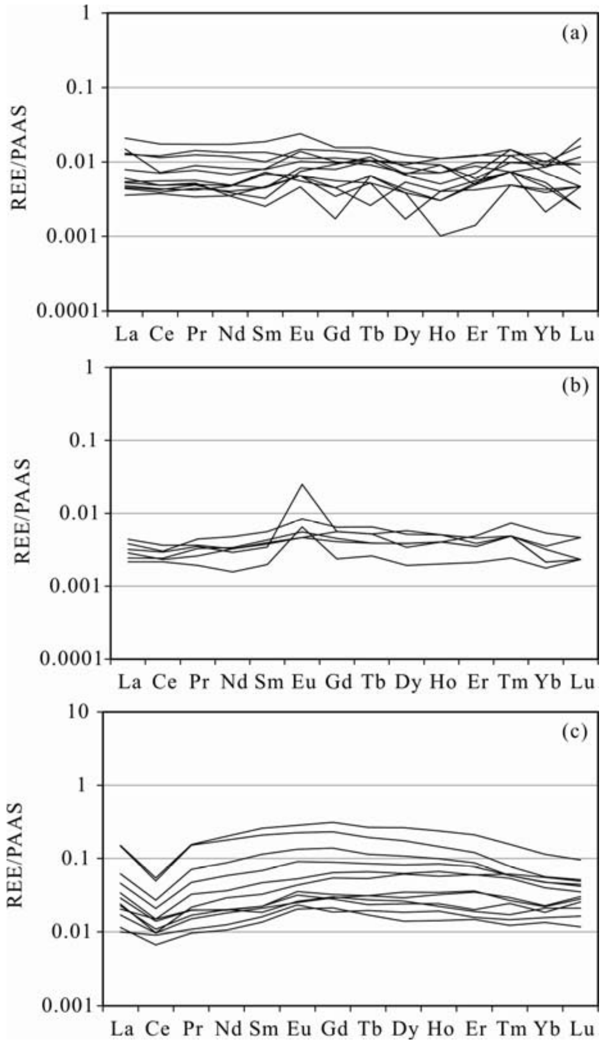

Fig. 7. REE distribution patterns for pore filling quartz(a), metasomatic chert(b) and host dolomite(c) in the Sichuan basin.

cement on the pores wall formed in a syn- or pene-contemporaneous seawater environment. During the uplift and exposure processes related to Tongwan movement, dolomite in the Dengying Formation was temporally covered by seawater due to short-term tectonic subsidence or a relative elevation of sea level. This immersion resulted in first filling and cementing, with fibrous radial aragonite formed in dissolution pores, and then formation of fibrous radial dolomite (Figs. 2a and 2b, Figs. 3a and 3b) as a result of dolomitisation (Machel and Mountjoy, 1986; Huang Zhicheng et al., 1997). During the burial stage following the Tongwan movement, dissolution pores were further mineralised with coarse crystalline dolomite (Figs. 2a and 2b, Figs.3a and 3b) of hydrothermal origin (Liu Shugen et al., 2008).

Pore-filling quartz commonly occurs in the spaces left behind coarse crystalline dolomite formation (Figs. 2a, 2b and 2d, Figs. 3a and 3b), suggesting that the quartz formed after the coarse crystalline dolomite. Pores and fractures filled with bitumen can be observed in the pore-filling quartz (Fig. 2d, Figs. 3b and 3g), indicating that bitumen formation occurred after the quartz formation. The widespread bitumen deposits in the dolomite reservoirs of the Dengying Formation were gradually derived from crude oil after extended deep burial and thermal evolution; therefore, oil entrapment occurred after quartz deposition.

The contact relationships between dolomite, quartz and bitumen suggest that the diagenetic sequence in order from first to last is fibrous radial dolomite, coarse crystalline dolomite, quartz and then bitumen.

5.2 Geochemical constraints on fluid features

5.2.1 Trace elements

In a trace element diagram normalised by upper continental crust values, the host dolomite values fall mostly below 1 (Fig. 6), indicating that the trace element concentrations are less than the average crustal values. This is a result of massive dolomitisation that generally occurs in seawater environments (Warren, 2000) wherein trace element concentrations are relatively low.

The pore-filling quartz and metasomatic chert are remarkably different from the host dolomite in not only their concentrations but also the distribution of trace elements (Fig. 6), indicating that the silica-rich fluid that precipitated quartz or caused replacement of dolomite by chert is different in composition from the seawater that formed the host dolomite. As shown in Fig. 6, there are clear differences between the quartz or metasomatic chert and the crustal average, suggesting that the silica-rich fluid did not originate from the crust.

Sr is a common element in dolomite and generally

Table 2 Concentrations of rare earth elements in host dolomite, pore-filling quartz and metasomatic chert in Sichuan basin and surrounding areas

Sample	Rare earth elements (ppm)														∑REE	LREE/HREE	δEu	δCe
	La	Ce	Pr	Nd	Sm	Eu	Gd	Tb	Dy	Ho	Er	Tm	Yb	Lu				
Pore-filling quartz																		
YK-1Qz	0.57	0.571	0.079	0.276	0.044	0.011	0.045	0.008	0.043	0.011	0.035	0.005	0.037	0.003	1.738	8.294	1.164	0.621
BMG-2Qz	0.798	1.39	0.152	0.584	0.104	0.026	0.073	0.012	0.058	0.011	0.034	0.006	0.028	0.007	3.283	13.336	1.405	0.921
JZ-2Qz	0.183	0.345	0.037	0.159	0.038	0.007	0.021	0.005	0.02	0.003	0.015	0.003	0.015	0.001	0.852	9.265	1.167	0.967
JZ-3Qz	0.201	0.384	0.044	0.163	0.04	0.006	0.021	0.002	0.025	0.004	0.012	0.002	0.011	0.002	0.917	10.608	0.975	0.942
HB-3Qz	0.503	0.913	0.11	0.401	0.056	0.016	0.066	0.01	0.04	0.007	0.025	0.003	0.024	0.005	2.179	11.106	1.239	0.896
YK-6Qz	0.167	0.312	0.039	0.137	0.025	0.007	0.026	0.004	0.018	0.003	0.014	0.003	0.013	0.001	0.769	8.378	1.293	0.892
YK-7Qz	0.207	0.44	0.05	0.166	0.025	0.009	0.037	0.008	0.046	0.009	0.014	0.005	0.02	0.002	1.038	6.362	1.393	0.998
BMG-2Qz	0.174	0.335	0.043	0.131	0.018	0.008	0.043	0.009	0.032	0.009	0.017	0.004	0.029	0.004	0.856	4.823	1.354	0.894
BMG-3Qz	0.3	0.559	0.068	0.227	0.045	0.015	0.047	0.007	0.033	0.007	0.028	0.004	0.026	0.004	1.370	7.782	1.536	0.903
LJC-1Qz	0.478	0.957	0.126	0.452	0.075	0.012	0.053	0.008	0.031	0.005	0.02	0.006	0.024	0.009	2.256	13.462	0.896	0.900
LJC-8Qz	0.137	0.298	0.03	0.119	0.026	0.007	0.016	0.004	0.008	0.004	0.016	0.003	0.006	0.002	0.676	10.458	1.616	1.072
LJC-9Qz	0.231	0.384	0.046	0.118	0.014	0.005	0.008	0.005	0.018	0.001	0.004	0.002	0.012	0.002	0.850	15.346	2.225	0.859
LJC-3	0.066	0.11	0.013	0.097	0.014	0.002	0.009	0.001	0.032	0.002	0.005	0.005	0.002	0.001	1.399	9.935	1.355	0.905
Average	0.329	0.574	0.069	0.244	0.043	0.011	0.038	0.007	0.031	0.006	0.020	0.004	0.020	0.004	1.738	8.294	1.164	0.621
Metasomatic chert																		
LJC-2C	0.109	0.184	0.023	0.11	0.022	0.005	0.019	0.003	0.018	0.004	0.01	0.002	0.006	0.001	0.516	7.190	1.152	0.848
LJC-6C	0.146	0.239	0.039	0.162	0.031	0.009	0.03	0.005	0.024	0.005	0.011	0.002	0.009	0.001	0.713	7.195	1.390	0.731
LJC-13C	0.093	0.191	0.029	0.114	0.024	0.006	0.021	0.003	0.018	0.004	0.01	0.002	0.006	0.001	0.522	7.031	1.258	0.849
ZY-7C	0.122	0.233	0.031	0.098	0.019	0.027	0.026	0.004	0.027	0.005	0.013	0.002	0.01	0.002	0.619	5.955	5.720	0.874
ZY-9C	0.082	0.171	0.017	0.053	0.011	0.007	0.011	0.002	0.009	0.002	0.006	0.001	0.005	0.001	0.378	9.216	2.997	1.057
YB-7C	0.168	0.29	0.032	0.11	0.021	0.005	0.026	0.004	0.016	0.004	0.014	0.003	0.015	0.002	0.710	7.452	1.008	0.913
Average	0.120	0.218	0.029	0.108	0.021	0.010	0.022	0.004	0.019	0.004	0.011	0.002	0.009	0.001	0.576	7.340	2.254	0.878
Host dolomite																		
HB-3	0.437	0.527	0.085	0.358	0.075	0.022	0.099	0.013	0.065	0.014	0.042	0.005	0.038	0.005	1.785	5.352	1.202	0.631
YK-1	0.915	0.774	0.19	0.982	0.18	0.047	0.252	0.041	0.287	0.057	0.172	0.022	0.112	0.015	4.046	3.223	1.039	0.428
YK-2	1.29	1.18	0.286	1.23	0.26	0.057	0.299	0.051	0.292	0.066	0.169	0.025	0.156	0.021	5.382	3.988	0.963	0.448
YK-4	0.648	0.762	0.133	0.614	0.117	0.027	0.135	0.024	0.162	0.034	0.103	0.011	0.062	0.012	2.844	4.238	1.012	0.599
BMG-1	1.1	1.11	0.173	0.677	0.102	0.028	0.139	0.021	0.123	0.022	0.054	0.007	0.059	0.009	3.624	7.350	1.107	0.587
YB-11	0.777	1.18	0.176	0.669	0.123	0.034	0.13	0.018	0.113	0.024	0.057	0.01	0.052	0.011	3.374	7.130	1.266	0.736
Ljc-3	5.65	3.94	1.34	6.08	1.16	0.243	1.08	0.149	0.818	0.144	0.343	0.032	0.159	0.022	21.160	6.703	1.022	0.330
Ljc-6	2.37	2.15	0.629	2.96	0.636	0.145	0.647	0.088	0.505	0.098	0.249	0.024	0.134	0.018	10.653	5.043	1.064	0.406
Ljc-7	1.75	1.65	0.415	1.98	0.381	0.098	0.413	0.065	0.383	0.083	0.221	0.024	0.133	0.019	7.615	4.679	1.163	0.447
Ljc-17	0.38	0.713	0.096	0.423	0.089	0.025	0.087	0.015	0.086	0.019	0.045	0.006	0.044	0.007	2.035	5.586	1.338	0.861
LJC-4	0.861	0.863	0.148	0.681	0.123	0.038	0.15	0.024	0.136	0.032	0.099	0.012	0.064	0.013	3.244	5.121	1.317	0.558
LJC-10	5.78	4.32	1.37	6.81	1.44	0.306	1.45	0.205	1.23	0.235	0.599	0.064	0.323	0.041	24.173	4.829	0.997	0.354
ZY-5	0.399	0.725	0.083	0.33	0.062	0.01	0.048	0.01	0.047	0.009	0.028	0.003	0.024	0.005	1.783	9.247	0.863	0.919
Average	1.720	1.530	0.394	1.830	0.365	0.083	0.379	0.056	0.327	0.064	0.168	0.019	0.105	0.015	7.055	5.576	1.104	0.562
PAAS*	38.2	79.6	8.83	33.9	5.55	1.08	4.66	0.77	4.68	0.99	2.85	0.41	2.82	0.43				

*PAAS, Post Archean Australian Shale, Taylor and McLennan (1985).

∑REE, Total concentration of rare earth elements; LREE/HREE, Concentration of light rare earth element / concentration of heavy rare earth element; $\delta Eu = Eu/\sqrt{Sm*Gd}$ N; $\delta Ce = Ce/\sqrt{La*Pr}$ N; N, normalized value by PAAS.

Table 3 Strontium, oxygen and hydrogen isotope compositions in host dolomite, pore-filling quartz and metasomatic chert in Sichuan basin and surrounding areas

Sample	$^{87}Sr/^{86}Sr$ (‰)	δD_{VSMOW} (‰)	$\delta^{18}O_{VSMOW}$ (‰)	Th (°C)	Fluid* $\delta^{18}O_{VSMOW}$ (‰)
Pore-filling quartz					
YH-2Qz	0.715668	-85.1	20.0		
YK-1Qz	0.716564	-63.6	23.1	166.8	8.5
BMG-2Qz	0.711082	-84.8	21.7	185.6	8.5
BMG-3Qz	0.712134	-63.1	20.8	185.6	7.6
JZ-3Qz	0.710528	-60.7	23.9		
YK-7Qz	0.711630	-53.2	23.4	147.8	7.2
BMG-3Qz	0.711100	-81.5	23.8	185.6	10.6
JZ-5Qz	0.711239	-53.1	23.5	146.4	7.2
LJC-1Qz	0.712434	-57.9	19.5		
LJC-8Qz	0.709171	-53.8	23.4		
LJC-9Qz	0.709068	-54.3	20.9	183.3	7.6
LJC-10Qz	0.709465	-67.8	21.7	183.3	8.3
LJC-3Qz	0.710540	-57.4	20.0	204.2	8.1
Average	0.711586	-64.3	22.0		8.2
Metasomatic chert					
LJC-2C	0.710306		25.0		
LJC-6C	0.709897		26.7		
LJC-12C	0.712375		23.7		
1-LJC-13C	0.709229		25.7		
ZY-7C	0.708970		28.1		
ZY-9C	0.709042		25.4		
YB-7C	0.709597		20.7		
Average	0.709917		25.0		
Host dolomite					
YH-2	0.709893				
HB-3	0.708887				
JZ-1	0.710583				
YK-1	0.709088				
YK-2	0.709510				
YK-4	0.709807				
BMG-1	0.709871				
BMG-2	0.708954				
BMG-5	0.709081				
YK-7	0.709289				
Average	0.709496				

*$\delta^{18}O_{VSMOW}$ values of inclusion fluid, parent fluid for quartz precipitation, were calculated according to $\delta^{18}O_{VSMOW}$ values of quartz, homogenization temperature (Th) and fractionation factor between fluid and quartz ($\alpha=3.38*10^6/T^2-2.90$, Zheng Yongfei and Chen Jiangfeng (2000)).

originates from seawater. However, the Sr concentrations in the pore-filling quartz and metasomatic chert are lower than in the host dolomite, suggesting that the relevant silica-rich fluid is not seawater-derived. Cr, Co, Mo, W and Fe are siderophile elements that are usually enriched in deep sialic crust. Enrichment of these elements in quartz and chert indicates that chemical and energy exchanges may have occurred between the silica-rich fluid and sialic crust, in which the silica-rich fluid obtained some of its siderophile element content.

5.2.2 Rare earth elements

The low rare earth element concentrations and negative Ce anomaly in the host dolomite were generally inherited from seawater during deposition (Webb et al., 2000; Hu Wenxuan, 2010; Nothdurft et al., 2004). In comparison with the host dolomite, the rare earth element concentrations in pore-filling quartz and metasomatic chert are relatively low and do not have negative Ce anomalies (Table 2; Fig. 7), suggesting that the quartz and chert did not precipitate from seawater.

Most of the pore-filling quartz and metasomatic chert samples have positive Eu anomalies and among them the samples LJC-9Qz, ZY-9Cand ZY-7C display δEu values of 2.23, 3.00 and 5.72, respectively.

Previous investigations have shown that despite large differences in rare earth element concentrations in different hydrothermal systems (Michard, 1989; Klinkhammer et al., 1994), rare earth element distribution patters are globally very similar in various hydrothermal fluids with consistent enrichment in light rare earth elements and positive Eu anomalies (Mills et al., 1995; James et al., 1996). Changes in Eu content are usually associated with changes in temperature and redox conditions. In a reducing environment at higher temperatures, Eu^{3+} is reduced to Eu^{2+} (Cai et al., 2008; Wang Xiaolin et al., 2009; Zhang Juntao et al., 2009) and the fluid Eu^{2+}/Eu^{3+} ratio is strongly controlled by temperature, which reaches a balance at 250° C (Sverjensky et al., 1984; Bau et al., 1992). Because the ionic radius of Eu^{2+} is greater than that of Eu^{3+} (0.117 vs 0.095 nm), Eu^{2+} is less able to enter rock-forming minerals than Eu^{3+} (Cai et al., 2008). Therefore, at high temperatures, Eu can become enriched in hydrothermal fluids in the form of Eu^{2+}. With decreasing temperature, the enriched Eu^{2+} gradually transforms into Eu^{3+}. Therefore, the related hydrothermal minerals, such as calcite, dolomite and quartz, can contain relatively high concentrations of Eu and positive Eu anomalies.

The positive Eu anomaly in the hydrothermal fluid was likely inherited by the precipitated quartz and metasomatic chert, resulting in a positive Eu anomaly in most of the quartz and chert samples (Table 2; Fig. 7).

5.2.3 Hydrogen and oxygen isotopes

The $\delta^{18}O_{SMOW}$ value of magmatic water in isotopic equilibrium with magma at high temperatures is generally between 6‰ and 9‰, and δD_{SMOW} is generally between −50‰ and −80‰ (Zheng Yongfei and Chen Jiangfeng, 2000). The $\delta^{18}O_{SMOW}$ value of metamorphic water is typically between +5‰ and +25‰, with δD_{SMOW} between −20‰ and −70‰ (Taylor, 1979). During burial and deep-burial diagenesis, the $\delta^{18}O_{SMOW}$ value of connate pore-water gradually increases due to water-rock interactions, but never reaches values above 3‰±1‰ (Longstaffe, 1987).

The hydrogen and oxygen isotope compositions of the silica-rich hydrothermal fluid that precipitated quartz in the Dengying Formation dolomite are considerably different from those of metamorphic water and connate pore water. The $\delta^{18}O_{SMOW}$ and δD_{SMOW} values of the silica

-rich hydrothermal fluid lie within the range for magmatic water (Fig. 8), suggesting that the silica-rich fluid was related to magmatic activity and that it experienced interaction and isotopic equilibrium with magma.

During precipitation from a parent fluid, the oxygen isotope composition of quartz is controlled by the fluid oxygen isotope composition and temperature and follows the thermodynamic equilibrium principle of isotope fractionation. However, the oxygen isotope composition of metasomatic chert is also affected by the dynamics of the metasomatism process. Compared with the pore-filling quartz, metasomatic chert is relatively heavy in its oxygen isotope composition. This can be explained by a kinetic isotope fractionation mechanism. The metasomatic reaction for dolomite replacement by chert is as follows (Chen Yongquan et al., 2010):

$$MgCa\ (CO_3)_2 + 2CO_2 + H_4SiO_4 = Mg\ (HCO_3)_2 + Ca\ (HCO_3)_2 + SiO_2 \quad (1)$$

This reaction is strongly affected by the acidity generated by ortho-silicic acid. For oxygen-containing acidic fluids, the acidity depends on the attraction of electrons by the core atoms: the greater the attraction, the greater the acidity. For a given element, the attraction of atoms to the surrounding electrons is positively proportional to the mass number of the isotopes. Compared to ^{16}O, ^{18}O has a stronger attraction to the surrounding electrons. Therefore, the distribution of the electronic cloud in H_4SiO_4 containing ^{18}O is more inclined to O, resulting in weaker H-^{18}O bonds than H-^{16}O bonds. This indicates that H-^{18}O bonds can be more easily broken to release hydrogen ions. Therefore, H_4SiO_4 containing ^{18}O has greater acidity and is more likely to dissolve and replace dolomite, consequently resulting in the formation of metasomatic chert with a heavier oxygen isotope composition.

In addition, the oxygen isotope composition of metasomatic chert is also controlled by temperature and the water/rock ratio during metasomatism. At lower metasomatic temperatures, metasomatism proceeds more slowly and more ^{18}O-containing H_4SiO_4 is selectively consumed, resulting in the formation of chert with a heavier oxygen isotope composition. Similarly, at higher water/rock ratios, even more ^{18}O-containing H_4SiO_4 is selectively consumed, resulting in the formation of chert with an even heavier oxygen isotope composition.

5.2.4 Strontium isotopes

The $^{87}Sr/^{86}Sr$ values in pore-filling quartz and metasomatic chert are higher than those in the host dolomite, suggesting that the silica-rich hydrothermal fluid had higher $^{87}Sr/^{86}Sr$ values.

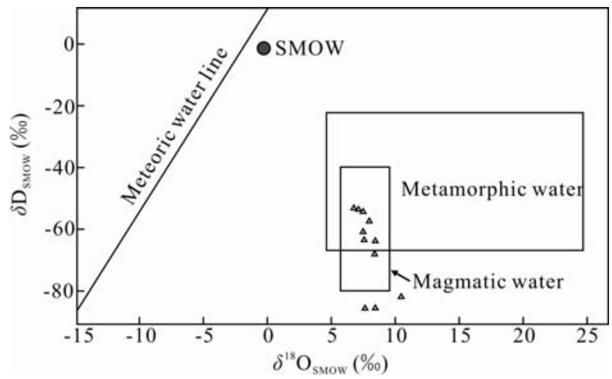

Fig. 8. Plot of hydrogen and oxygen isotopes for fluid precipitating quartz in the Sichuan Basin and surrounding areas. Most of the pore-filling quartz samples are in the scope of magmatic water, suggesting that the fluid was in equilibrium with magma in oxygen and hydrogen isotopes.

^{87}Sr is generally derived from the decay of radioactive Rb, and its abundance changes with time and location. ^{86}Sr does not originate from radioactive elements and its abundance is relatively constant. Felsic clastic rocks and mudstones usually contain more radiogenic ^{87}Sr and display higher $^{87}Sr/^{86}Sr$ values. For example, $^{87}Sr/^{86}Sr$ values in silicate clastic materials separated from the late Cenozoic sediments on the Alpha ridge in the central Atlantic Ocean are between 0.713100 and 0.725100 (Winter et al., 1997).

During upward migration along faults and fractures, silica-rich hydrothermal fluids react with the underlying siliceous clastic sediments to achieve high $^{87}Sr/^{86}Sr$ values (Davies and Smith, 2006; Cai et al, 2008). The $^{87}Sr/^{86}Sr$ value of the pore-filling quartz precipitated from a silica-rich hydrothermal fluid is consequently high. During metasomatism of dolomite by the silica-rich hydrothermal fluid, the lower $^{87}Sr/^{86}Sr$ value of dolomite was partially retained in metasomatic chert. As a result, the $^{87}Sr/^{86}Sr$ values of the metasomatic chert are intermediate between those of the pore-filling quartz and the host dolomite.

5.3 Fluid inclusions

According to Tissot's classic model for hydrocarbon generation from kerogens (Tissot et al., 1974), kerogen ceases to produce oil at burial depths greater than 4000 m (R_o>1.3%). The geothermal gradient during the evolution of the Sichuan Basin was approximately 30°C/km (Wang Yanfei and Xiao Xianming, 2010). Based on this figure, the temperature in the formation at a burial depth of 4000 m was estimated to be about 140°C. The hydrocarbon source rocks in the Z_2dy^3 and Lower Cambrian likely ceased oil generation when the burial temperatures reached 140°C.

Because the pore-filling quartz formed prior to oil entrapment, the temperature of the host Dengying

Formation dolomite during quartz precipitation is expected to be lower than or near the temperatures present during hydrocarbon accumulation (about 140° C). However, the temperatures determined for most fluid inclusions in quartz are consistently above 140°C and reach as high as 228.3° C, indicating that fluid temperatures during quartz precipitation were greater than the ambient temperature in the surrounding dolomite; therefore, the precipitating fluid was a typical hydrothermal fluid (Machel and Lonnee 2002; Davies and Smith, 2006).

The gases in fluid inclusions in pore-filling quartz are mainly CO_2, CH_4 and N_2, which are gases that are commonly released during volcanic eruptions and hot springs (Gerlach, 1980; Shangguan Zhiguan et al., 2000; Forrest et al., 2005; Lollar et al., 2008).

5.4 Mechanisms of silica-rich hydrothermal fluid migration

The results of elemental composition, isotopic composition and fluid inclusion analyses indicate that the formation of pore-filling quartz and metasomatic chert can be attributed to the activity of silica-rich hydrothermal fluids.

Silica-rich hydrothermal fluids can form by dissolving SiO_2 in an alkaline environment. In hot springs on ocean ridges (Douvill et al., 2002; Proskurowski et al., 2006; Charlou et al., 2010; Schmidt et al., 2011), continent interiors (Blank et al., 2009) and Precambrian shields (Lollar et al., 2008; McCollom, 2013; Sephton and Hazen 2013), olivine and pyroxene in basic rocks have been shown to serpentinise in reactions with water, forming a reduced and high-pH environment with hydrothermal fluids that usually contain some SiO_2 (Schrenk et al., 2013). In reduced and high-temperature springs, H_2, CO_2 and CO can combine to generate CH_4 through Fischer–Tropsch-type synthesis (Charlou et al., 2002; Proskurowski et al., 2006; McCollom, 2013).

Oil and gas in the Sinian Dengying Formation reservoirs in the Sichuan Basin and adjacent areas mainly originated from Lower Cambrian black shales. The hydrocarbon generation peak occurred during the middle and late Caledonian orogeny (Ordovician to Silurian) (Zhao Zongju et al., 2003; Li Shuangjian et al., 2011). Based on the observed mineralogical relationships that indicate that pore-filling quartz and metasomatic chert formed prior to oil (bitumen) emplacement, the silica-rich hydrothermal fluid might be related to hydrothermal activity earlier than the Ordovician. A study by Chen et al. (2009) confirmed that silica-rich hydrothermal activity occurred during the early Cambrian.

The hydrogen isotopic compositions of hydrothermal fluid are mainly determined by the hydrogen isotopic composition of the original fluid. The hydrogen isotopic composition of hydrothermal fluids formed by deep circulation of seawater is close to that of seawater. For instance, the δD_{SMOW} values for vent fluids from the southern Juan de Fuca Ridge are −2.5‰ to 0.5‰ (Shanks and William, 1987). The hydrogen isotopic composition of hydrothermal fluid derived from deep circulation of meteoric water is generally light (Marques et al., 2008). The δD_{SMOW} values of fluid inclusions in the pore-filling quartz range from −85.1‰ to −53.1‰ with an average of −64.3‰. The light hydrogen isotope composition indicates a deep-circulating meteoric water source for the silica-rich hydrothermal fluid.

A silica-rich hydrothermal process is proposed here for the Sichuan Basin and its adjacent areas (Fig. 9). During the early Cambrian, meteoric water was cycled deep underground along basement faults wherein it formed hydrothermal fluids after heating by basement rocks. Serpentinisation and Fischer–Tropsch type synthesis in the deep basement generated and released gases such as CO_2 and N_2, and some alkane components such as CH_4. High-pH hydrothermal fluids resulting from serpentinisation then dissolved SiO_2 from the surrounding rocks to produce a silica-rich hydrothermal fluid. When the silica-rich hydrothermal fluid containing various gaseous components entered shallow strata, such as the Dengying Formation dolomite, silicon was precipitated in response to the lower temperatures and pH, forming pore-filling quartz or metasomatic chert through dolomite replacement.

5.5 Influence on dolomite reservoir

Chen Yongquan et al. (2010) argued that silica-rich hydrothermal fluids can dissolve carbonate rocks to improve reservoir quality. However, the main effect of silica-rich hydrothermal activity on dolomite reservoirs is to reduce the reservoir porosity, resulting in densification of the dolomite reservoir. Petrological and mineralogical observations show that dolomite crystals in quartz-filled pores display fewer signs of dissolution. Presence of CO_2 in the silica-rich fluid may increase its ability to dissolve dolomite reservoir.

We speculate that the silica-rich hydrothermal fluids did not completely destroy the dolomite reservoir spaces and left many remaining pores (Figs. 2b, 2c and 2d), which currently act as the main storage spaces for natural gas. In addition, siliceous deposition (quartz) and metasomatism (chert) further increased the ability of the reservoir rock framework to resist compression and reduced the amount of compaction and pressure solution, which was a significant factor in the retention of pores during

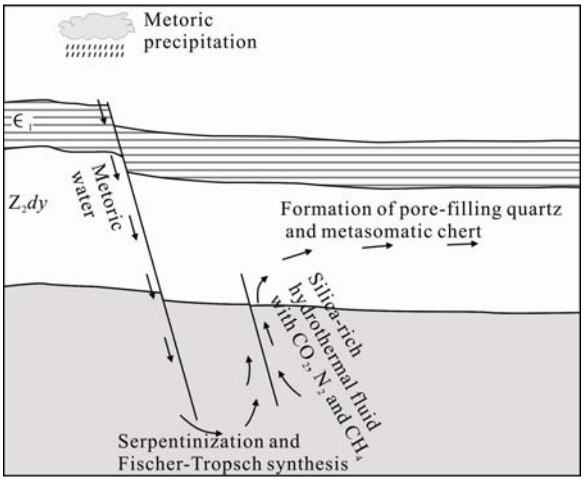

Fig. 9. Evolution model for silica-rich hydrothermal fluid.
After precipitation, meteoric water flowed downwards along fault and then was heated by magma in deep strata. The heated meteoric water became hydrothermal fluid migrating upwards. The hydrothermal fluid could dissolve SiO_2 through interaction with deep rocks and capture gas components that might be product of serpentinization or Fischer-Tropsch type synthesis.

subsequent deep burial.

6 Conclusions

(1) Pore-filling quartz and metasomatic chert in the dolomite of the Sinian Dengying Formation in the Sichuan Basin and surrounding areas were formed after the pore-filling dolomite but before oil (bitumen) entrapment.

(2) The compositions of trace element, rare earth element and hydrogen, oxygen and strontium isotope along with fluid inclusion compositions indicate that the formation of quartz and chert was associated with the activity of silica-rich hydrothermal fluids derived from deep-circulating meteoric water along basement faults.

(3) Quartz precipitation and siliceous metasomatism resulted in densification of the dolomite reservoirs in the Dengying Formation but increased its resistance to compaction, which in turn improved the ability of the reservoir to maintain pore spaces.

(4) Evidence for deep circulation of meteoric water along basement faults and related silica-rich hydrothermal activity are common in the Yangtze Platform and Tarim Basin and their influence on deep dolomite reservoirs should be thoroughly considered.

Acknowledgements

This work was financially supported by the National Natural Science Foundation of China (grants No. 41372149, 41625009, 41230312 and U1663209) and the Strategic Priority Research Program of the Chinese Academy of Science (grant No. XDA14010201).

Manuscript received Dec. 15, 2015
accepted Feb. 6, 2017
edited by Hao Qingqing

References

Bau, M., and Möller, P., 1992. Rare earth element fractionation in metamorphogenic hydrothermal calcite, magnesite and siderite. *Mineralogy and Petrology,* 45(3–4): 231–246.

Blank, J.G., Green, S.J., Blake, D., Valley, J.W., Kita, N.T., Treiman, A., and Dobson, P.F., 2009. An alkaline spring system within the Del Puerto Ophiolite (California, USA), A Mars analog site. *Planetary and Space Science,* 57(5–6): 533–540.

Breesch, L., Swennen, R., Vincent, B., Ellison, R., and Dewever, B., 2010. Dolomite cementation and recrystallisation of sedimentary breccias along the Musandam Platform margin (United Arab Emirates). *Journal of Geochemical Exploration,* 106(1–3): 34–43.

Cai Chunfang, Li Kaikai, Li Hongtao and Zhang Baoshu, 2008. Evidence for cross formational hot brine flow from integrated $^{87}Sr/^{86}Sr$, REE and fluid inclusions of the Ordovician veins in Central Tarim, China. *Applied Geochemistry,* 23(8): 2226–2235.

Charlou, J.L., Donval, J.P., Fouquet, Y., Jean-Baptiste, P., and Holm, N., 2002. Geochemistry of high H_2 and CH_4 vent fluids issuing from ultramafic rocks at the Rainbow hydrothermal field (36°14′N, MAR). *Chemical Geology*, 191(4): 345–359.

Charlou, J.L., Donval, J.P., Konn, C., Ondréas, H., and Fouquet, Y., 2010. High production and fluxes of H_2 and CH_4 and evidence of abiotic hydrocarbon synthesis by serpentinization in ultramafic-hosted hydrothermal systems on the Mid-Atlantic Ridge. In: Rona, P.A., Devey, C.W., Dyment, J., and Murton, B.J., (eds), *Diversity of Hydrothermal Systems on Slow Spreading Ocean Ridges*. Washington D. C.: American Geophysical Union, 265–296.

Chen Daizhao, Wang Jianguo, Qing Hairuo, Yan Detian and Li Renwei, 2009. Hydrothermal venting activities in the early Cambrian, south China, petrological, geochronological and stable isotopic constraints. *Chemical Geology,* 258(3–4): 168–181.

Chen Yongquan, Jiang Shaoyong, Zhou Xinyuan, Yang Wenjing and Han Lijun, 2010. δ^{30}Si, δ^{18}O and elements geochemistry on the bedded siliceous rocks and cherts in dolostones from Cambrian strata, Tarim Basin. *Geochimica,* 39(2): 159–170 (in Chinese with English abstract).

Davies, G.R., and Smith, L.B., 2006. Structurally controlled hydrothermal dolomite reservoir facies, an overview. *AAPG Bulletin,* 90(11): 1641–1690.

Douvill, E., Charlou, J.L., Oelkers, E.H., Bienvenu, P., Colon, C.F.J., Donval, J.P., Fouquet, Y., Prieur, D., and Appriou, P., 2002. The rainbow vent fluids (36 degrees 14′N, MAR), the influence of ultramafic rocks and phase separation on trace metal content in Mid-Atlantic Ridge hydrothermal fluids. *Chemical Geology,* 184(1–2): 37–48.

Ehrenberg, S.N., 2006. Porosity destruction in carbonate platforms. *Journal of Petroleum Geology,* 29(1): 41–52.

Forrest, M.J., Jorge, L.V., William, U.III, Justin, T.K., and David, R.H., 2005. Gas geochemistry of a shallow submarine hydrothermal vent associated with the El Requesón fault zone, Bahía Concepción, Baja California Sur, México. *Chemical Geology,* 224(1): 82–95.

Gerlach, T.M., 1980. Evaluation of volcanic gas analyses from Kilauea volcano. *Journal of Volcanology and Geothermal Research,* 7(3–4): 295–317.

Hao Fang, Zhang Xuefeng, Wang Cunwu, Li Pingping, Guo Tonglou, Zou Huayao, Zhu Yangming, Liu Jianzhang and Cai Zhongxian, 2015. The fate of CO_2 derived from thermochemical sulfate reduction (TSR) and effect of TSR on carbonate porosity and permeability, Sichuan Basin, China. *Earth-Science Reviews*, 141: 154–177.

Hu Wenxuan, Chen Qi, Wang Xiaolin and Cao Jian, 2010. REE models for the discrimination of fluids in the formation and evolution of dolomite reservoirs. *Oil and Gas Geology,* 31(6): 810–818 (in Chinese with English abstract).

Huang Keke, Zhong Yijiang, Huang Sijing, Li Xiaoning and Feng Mingshi, 2016. Saddle-dolomite-bearing fracture fillings and records of hot brine activity in the Jialingjiang Formation, Libixia section, Hechuan area of Chongqing City. *Acta Geologica Sinica* (English Edition), 90(1): 195–208.

Huang Zhicheng, Yang Shouye and Chen Zhina, 1997. Mineralogical correlation between primary and replacement dolomites. *Science China Series D-Earth Sciences,* 40 (1): 91–98.

James, R.H., and Henry, E., 1996. Chemistry of ore-forming fluids and mineral formation rates in an active hydrothermal sulfide deposit on the Mid-Atlantic Ridge. *Geology,* 24(12): 1147–1150.

Jin Zhijun, 2005. Particularity of petroleum exploration on marine carbonate strata in China sedimentary basin. *Earth Science Frontier,* 12(3): 15–22 (in Chinese with English abstract).

Jin Zhijun, Zhu Dongya, Zhang Xuefeng, Hu Wenxuan and Song Yucai, 2006. Hydrothermally fluoritized Ordovician carbonates as reservoir rocks in the Tazhong area, NW China. *Journal of Petroleum Geology,* 29(1): 27–40.

Jin Zhijun, Zhu Dongya, Hu Wenxuan, Zhang Xuefeng and Zhang Juntao, 2009. Mesogenetic dissolution of the middle Ordovician limestone in the Tahe oilfield of Tarim Basin, NW China. *Marine and Petroleum Geology,* 26(6): 753–763.

Klinkhammer, G.P., Elderfield, H., Edmond, J.M., and Mitra, A., 1994. Geochemical implications of rare earth element patterns in hydrothermal fluids from mid-ocean ridges. *Geochimica et Cosmochimica Acta,* 58(23): 5105–5113.

Lavoie, D., Chi, G., Urbatsch, M., and Davis W.J., 2010. Massive dolomitization of a pinnacle reef in the Lower Devonian West Point Formation (Gaspé Peninsula, Quebec), An extreme case of hydrothermal dolomitization through fault -focused circulation of magmatic fluids. *AAPG Bulletin,* 94 (4): 513–531.

Li Shuangjian, Gao Bo, Wo Yujin, Zhou Yan and Yuan Yusong, 2011. Destruction types and temporal-spatial distribution of marine hydrocarbon reservoirs in South China. *Petroleum Geology and Exploration,* 33(1): 43–55 (in Chinese with English abstract).

Liu Quanyou, Worden, R.H., Jin Zhijun, Liu Wenhui, Li Jian, Gao Bo, Zhang Dianwei and Hu Anping, 2013. TSR versus non-TSR processes and their impact on gas geochemistry and carbon stable isotopes in Carboniferous, Permian and Lower Triassic marine carbonate gas reservoirs in the Eastern Sichuan Basin, China. *Geochimica et Cosmochimica Acta*, 100: 96–115.

Liu Quanyou, Zhu Dongya, Jin Zhijun, Liu Chunyan, Zhang Dianwei and He Zhiliang, 2016. Coupled alteration of hydrothermal fluids and thermal sulfate reduction (TSR) in ancient dolomite reservoirs–An example from Sinian Dengying Formation in Sichuan Basin, southern China. *Precambrian Research*, 285: 39–57.

Liu Shugen, Huang Wenming, Chen Cuihua and Zhang Changjun, 2008. Primary study on hydrothermal fluid activities and its effectiveness on petroleum and mineral accumulation of Sinian system – Paleozoic in Sichuan Basin. *Journal of Mineralogy and Petrology,* 28(3): 41–50 (in Chinese with English abstract).

Liu Shugen, Huang Wenming, Jansa, L.F., Wang Guozhi, Song Guangyong, Zhang Changjun, Sun Wei and Ma Wenxin, 2014. Hydrothermal dolomite in the Upper Sinian (Upper Proterozoic) Dengying Formation, East Sichuan Basin, China. *Acta Geologica Sinica* (English Edition), 88(5): 1466–1487.

Liu, S.G, Qin, C., Jansa, L., Sun, W., Wang, G.Z., Xu, G.S., and Yuan, H.F., 2011. Transformation of oil pools into gas pools as results of multiple tectonic events in Upper Sinian (Upper Neoproterozoic), deep part of Sichuan Basin, China. *Energy, Exploration & Exploitation,* 29(6): 679–698.

Lollar, B.S., Lacrampe-Couloume, G., Voglesonger, K., Onstott, T.C., Pratt, L.M., and Slater, G.F., 2008. Isotopic signatures of CH_4 and higher hydrocarbon gases from Precambrian Shield sites, A model for abiogenic polymerization of hydrocarbons. *Geochimica et Cosmochimica Acta,* 72(19): 4778–4795.

Longstaffe, F.J., 1987. Stable isotope studies of digenetic processes. In: Kyser, T.K., (Ed.), *Stable Isotope Geochemistry at Low Temperature Fluids, MAC Short Course Series 13*. Québec: Mineralogical Association of Canada, 187–257.

Luo Zhili, 1981. Effects of rift activities from later Paleozoic on petroleum and other deposits in Southwestern China. *Journal of Sichuan Geology,* 2(1): 1–22 (in Chinese with English abstract).

Machel, H.G., and Lonnee, J., 2002. Hydrothermal dolomite – a product of poor definition and imagination. *Sedimentary Geology,* 152: 163–171.

Machel, H.G., and Mountjoy, E.W., 1986. Chemistry and environments of dolomitization — a reappraisal. *Earth-Science Reviews,* 23(3): 175–222.

Marques, J.M., Paula, M.C., Maria, R.C., Maria, J.M., Fraser, E.G., Maria, J.B., Rui, C.G., Luís, A.B., and Luís, R., 2008. Origins of high pH mineral waters from ultramafic rocks, Central Portugal. *Applied Geochemistry,* 23(12): 3278–3289.

Mazzullo, S.J., and Harris, P.M., 1992. Mesogenetic dissolution, its role in porosity development in carbonate reservoir. *AAPG Bulletin,* 76(5): 607–620.

McCollom, T.M., 2013. Laboratory simulations of abiotic hydrocarbon formation in Earth's deep subsurface. *Reviews in Mineralogy and Geochemistry,* 75: 467–494.

Michard, A., 1989. Rare earth element systematics in hydrothermal fluids. *Geochimica et Cosmochimica Acta,* 53 (3): 745–750.

Mills, R.A., and Henry, E., 1995. Rare earth element geochemistry of hydrothermal deposits from the active TAG Mound, 26 N Mid-Atlantic Ridge. *Geochimica et Cosmochimica Acta,* 59(17): 3511–3524.

Ni, Y.Y., Liao, F.R., Dai, J.X., Zou, C.N., Wu, X.Q., Zhang, D.J., Wang, T.S., 2014. Studies on gas origin and gas source correlation using stable carbon isotopes -A case study of the giant gas fields in the Sichuan Basin, China. *Energy,* *Exploration & Exploitation,* 32(1): 41–74.

Nothdurft, L.D., Gregory, E.W., and Balz, S.K., 2004. Rare earth element geochemistry of Late Devonian reefal carbonates, Canning Basin, Western Australia, confirmation of a seawater REE proxy in ancient limestones. *Geochimica et Cosmochimica Acta,* 68(2): 263–283.

Proskurowski, G., Marvin, D.L., Deborah, S.K., and Eric, J.O., 2006. Low temperature volatile production at the Lost City Hydrothermal Field, evidence from a hydrogen stable isotope geothermometer. *Chemical Geology,* 229(4): 331–343.

Qian Yixiong, Chen Yue, Chen Qianglu and You Donghua, 2006. General characteristics of burial dissolution for Ordovician carbonate reservoirs in the northwest of Tazhong area. *Acta Petrolei Sinica,* 27(3): 47–52 (in Chinese with English abstract).

Schmidt, K., Garbe-Schönberg, D., Koschinsky, A., Strauss, H., Jost, C.L., Klevenz, V., and Königer, P., 2011. Fluid elemental and stable isotope composition of the Nibelungen hydrothermal field (8 18′S, Mid-Atlantic Ridge), Constraints on fluid-rock interaction in heterogeneous lithosphere. *Chemical Geology,* 280(1): 1–18.

Schrenk, M.O., William, J.B., and Susan, Q.L., 2013. Serpentinization, carbon, and deep life. *Reviews in Mineralogy Geochemistry,* 75(1): 575–606.

Sephton, M.A., and Hazen, R.M., 2013. On the origins of deep hydrocarbons. *Reviews in Mineralogy and Geochemistry,* 75 (1): 449–465.

Shangguan Zhiguan, Bai Chunhua and Sun Mingliang, 2000. Mantle-derived magmatic gas releasing features at the Rehai area, Tengchong couty, Yunnan Province, China. *Science China Series D – Earth Sciences,* 43(2): 132–140.

Shanks, W.C., and William, E.S., 1987. Stable isotope studies of vent fluids and chimney minerals, southern Juan de Fuca Ridge, Sodium metasomatism and seawater sulfate reduction. *Journal of Geophysical Research Solid Earth*, 92(B11): 11387 –11399.

Shen Anjiang, Hu Anping, Pan Liyin and She Min, 2017. Origin and distribution of grain dolostone reservoirs in the Cambrian Longwangmiao Formation, Sichuan Basin, China. *Acta Geologica Sinica* (English Edition), 91(1): 204–218.

Sverjensky, D.A., 1984. Europium redox equlibria in aqueous solution. *Earth and Planetary Science Letters,* 67(1), 70–78.

Taylor, H.P.Jr., 1979. Oxygen and hydrogen isotope relationships in hydrothermal mineral deposits. In: Barnes, H.L. (Ed.), *Geochemistry of hydrothermal ore deposits* (2nd Edition). New York: John Wiley & Son, 236–277.

Taylor, S.R., and McLennan, S., 1985. *The Continental Crust: Its Composition and Evolution*. Oxford: Blackwell, 312.

Tissot, B., Durand, B., Espitalie, J., and Combaz, A., 1974. Influence of nature and diagenesis of organic matter in formation of petroleum. *AAPG Bulletin,* 58(3): 499–506.

Wang Xiaolin, Jin Zhijun, Hu Wenxuan, Zhang Juntao, Qian Yixiong, Zhu Jingquan and Li Qing, 2009. Using in situ REE analysis to study the origin and diagenesis of dolomite of Lower Paleozoic, Tarim Basin. *Science in China Series D-Earth Sciences*, 52(5): 681–693.

Wang Yanfei and Xiao Xianming, 2010. An investigation of Paleogeothermal gradients in the northeastern part of Sichuan Basin. *Marine Original Petroleum Geology,* 15(4): 57–61 (in Chinese with English abstract).

Warren, J., 2000. Dolomite, Occurrence，evolution and economically important associations. *Earth Science Reviews,* 52(1–3): 1–81.

Webb, G.E., and Balz, S.K., 2000. Rare earth elements in Holocene reefal microbialites, a new shallow seawater proxy. *Geochimica et Cosmochimica Acta,* 64(9): 1557–1565.

Wei, G.Q., Cheng, G.S., Du, S.M., Zhang, L., and Yang, W., 2008. Petroleum systems of the oldest gas field in China, Neoproterozoic gas pools in the Weiyuan gas field, Sichuan Basin. *Marine and Petroleum Geology,* 25(4–5): 371–386.

Winter, B.L., Johnson, C.M., and Clark, D.L., 1997. Strontium, neodymium, and lead isotope variations of authigenic and silicate sediment components from the Late Cenozoic Arctic Ocean, Implications for sediment provenance and the source of trace metals in seawater. *Geochimica et Cosmochimica Acta,* 61(19): 4181–4200.

Yin Xueqin, Li Peng and Li Daoling, 2015. Characteristics of occurrence and structure of the Ordovician siliceous rock in the Tabei area. *Geological Review*, 61(s): 760–761 (in Chinese with English abstract).

Zhang Juntao, Hu Wenxuan, Qian Yixiong, Wang Xiaolin, Cao Jian, Zhu Jingquan, Li Qing and Xie Xiaomin, 2009. Formation of saddle dolomites in Upper Cambrian carbonates, western Tarim Basin (northwest China): Implications for fault -related fluid flow. *Marine and Petroleum Geology*, 26(8): 1428–1440.

Zhang, S.N., Qing, H.R., and Meng, X.H., 2009. Petrography and geochemistry of the Cambrian dolomite reservoirs in Tarim Basin NW China, A case study based on deep cores sampled at depths of 7200–8500 m. *Journal of Geochemical Exploration,* 101(1): 123–123.

Zhao Zongju, Zhu Yan, Deng Hongying and Xu Yunjun, 2003. Control of paleo-uplift to the Meso-Paleozoic primary oil and gas pools in the south of China. *Petroleum Geology and Exploration,* 25(1): 10–17 (in Chinese with English abstract).

Zheng Yongfei and Chen Jiangfeng, 2000. *Stable isotope geochemistry*. Beijing: Science Press, 144–192 (in Chinese).

Zhu Dongya, Jin Zhijun and Peng Yongmin, 2013. Geochemical characteristics and differences of highly matured bitumen in the Sinian Dengying Formation. *Natural Gas Geoscience,* 24 (2): 382–387 (in Chinese with English abstract).

Zhu Dongya, Liu Quanyou, Jin Zhijun, Meng Qingqiang and Hu Wenxuan, 2017. Effects of deep fluids on hydrocarbon generation and accumulation in Chinese petroliferous basins. *Acta Geologica Sinica* (English Edition), 91(1): 301–319.

Zhu Dongya, Meng Qingqiang, Jin Zhijun, Liu Quanyou and Hu Wenxuan, 2015. Formation mechanism of deep Cambrian dolomite reservoirs in the Tarim basin, northwestern China. *Marine and Petroleum Geology*, 59(1): 232–244.

About the first author

ZHU Dongya, male, born in October 1975 in Shangqiu County, Henan Province, China; Doctor; He is now a senior engineer in Petroleum Exploration and Production Research Institute of SINOPEC and interested in carbonate sedimentary geology and reservoir. E-mail: zhudy.syky@sinopec.com. Tel., 010-82311152.